Feasibility study of wave-motion milling of carbon fiber reinforced plastic holes

OPEN ACCESS
IOP Publishing | IMMT
International Journal of Extreme Manufacturing
Int. J. Extrem. Manuf. 3 (2021) 010401 (13pp)
https://doi.org/10.1088/2631-7990/abc675

Editorial

Feasibility study of wave-motion milling of carbon fiber reinforced plastic holes

Deyuan Zhang[1,2,3], **Zhenyu Shao**[1,2], **Daxi Geng**[1,2,3], **Xinggang Jiang**[1,2,3], **Yihang Liu**[1,2], **Zehua Zhou**[1,2] and **Shaomin Li**[1,2]

[1] *School of Mechanical Engineering and Automation, Beihang University, Beijing 100191, People's Republic of China*

[2] *The Institute of Bionic and Micro-Nano Systems, Beihang University, Beijing 100191, People's Republic of China*

[3] *Beijing Advanced Innovation Center for Biomedical Engineering, Beihang University, Beijing 100191, People's Republic of China*

E-mail: gengdx@buaa.edu.cn

Abstract

Carbon fiber reinforced plastic (CFRP) has been applied in aeronautics, aerospace, automotive and medical industries due to its superior mechanical properties. However, due to its difficult-to-cut characteristic, various damages in twist drilling and chip removal clog in core drilling could happen, inevitably reducing hole quality and hole-manufacturing efficiency. This paper proposes the wave-motion milling (WMM) method for CFRP hole-manufacturing to improve hole quality. This paper presents a motion path model based on the kinematics of the WMM method. The wave-motion cutting mode in WMM was analyzed first. Then, comparison experiments on WMM and conventional helical milling (CHM) of CFRP were carried out under dry conditions. The results showed that the hole surface quality of the CFRP significantly improved with a decrease of 18.1%–36% of Ra value in WMM compared to CHM. WMM exerted a significantly weaker thrust force than that of CHM with a reduction of 12.0%–24.9% and 3%–7.7% for different axial feed per tooth and tangential feed per tooth, respectively. Meanwhile, the hole exit damages significantly decreased in WMM. The average tear length at the hole exit in WMM was reduced by 3.5%–29.5% and 35.5%–44.7% at different axial feed per tooth and tangential feed per tooth, respectively. Moreover, WMM significantly alleviated tool wear. The experimental results suggest that WMM is an effective and promising strategy for CFRP hole-manufacturing.

Keywords: carbon fiber reinforced plastic, wave-motion milling, cutting force, surface integrity

1. Introduction

Carbon fiber reinforced plastic (CFRP) has been applied in aeronautics, aerospace, automotive, medical and other manufacturing industries for its attractive properties, such as high stiffness and strength to weight ratio, excellent flexibility in designing and corrosion resistance [1–4]. Applying CFRP instead of conventional metal alloys not only reduces fuel consumption for environmental and economic purposes, but also improves durability and safety [5]. For instance, composites accounts for up to ∼57% of the primary structures found in the Boeing 787 (Dreamer-liner). Compared to other wide-body airplanes, the high proportion of composites in the Boeing 787 improves fuel efficiency by 15%–20% [6].

To meet assembly requirements, numerous highly precise holes need to be machined on CFRP parts. Conventional twist drilling remains the most widely

2631-7990/21/010401+13$33.00

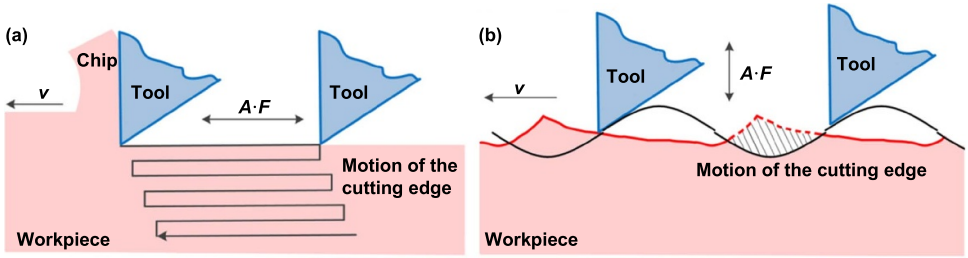

Figure 1. Schematic illustration of (a) convention ultrasonic vibration cutting mode and (b) wave-motion cutting mode [16].

applied process for CFRP hole-manufacturing. However, various damages can happen during twist drilling of CFRP, such as delamination and tearing, resin depletion, surface cavities, fuzzing, hole-roundness errors, thermal damage. Damages usually occur due to the heterogeneous and anisotropic nature of CFRPs [7–9]. These undesirable drilling-induced damages inevitably reduce the fatigue strength of the hole, weakening the long-term performance of machined CFRP parts [10]. Therefore, machining high quality and precise CFRP holes remains a challenge.

Recently, ultrasonic vibration-assisted machining has been applied in hole manufacturing of CFRP [11–14]. Ning *et al* [13] conducted an experimental study on rotary ultrasonic machining (RUM) of CFRP under pumped coolant. The results showed that compared to core drilling, RUM achieved higher hole quality with lower cutting force and torque. Cong *et al* [15] reported a comparison study on twist drilling and RUM of CFRPs under pumped coolant. The results showed that compared with twist drilling of CFRP, RUM has lower cutting force and smaller torque, less surface roughness, and longer tool life. However, pumped coolant increases the risk of hole exit delamination in core drilling. The inadvisable wet processing in aircraft assembly can have detrimental effects, such as moisture absorption on the shear fracture toughness of CFRP, making the wide application of RUM in aircraft assembly harder.

Wave-motion cutting is a novel hybrid machining method that has been applied in high-speed turning of titanium alloy by Sui *et al* [16], grinding of CFRP by Geng *et al* [3, 17] and high-speed side milling of titanium alloys by Liu *et al* [18]. As opposed to conventional ultrasonic vibration cutting where ultrasonic vibration is applied parallel to the cutting speed, the ultrasonic vibration is applied perpendicular to the cutting speed in wave-motion cutting, as shown in figure 1. A separate cutting mode (see figure 1) can be achieved in wave-motion cutting. Another advantage of wave-motion cutting is that the separated cutting mode can also be achieved at high cutting speeds instead of at the low cutting speed limit ($v_c < 2\pi f$) of conventional ultrasonic vibration cutting [16]. In order to eliminate drilling-induced damages during the twist drilling of CFRP, this paper proposed wave-motion milling (WMM), a novel hybrid process of CFRP hole-manufacturing, based on wave-motion cutting. The WMM process combines conventional helical milling (CHM) and ultrasonic machining, where an axial ultrasonic vibration is applied on the cutting edges when the tool rotates along its own axis and helical motion feeds into the workpiece. This paper first provides a comprehensive review of the machinability of CFRP holes by the WMM method and it reports the results from comparative experiments of WMM and CHM of CFRP. Cutting behaviors were evaluated by observing and comparing several output parameters, including hole surface integrity, thrust force, delamination at hole exit, and hole and tool wear. Additionally, cutting force reduction, delamination formation and suppression in WMM were also analyzed.

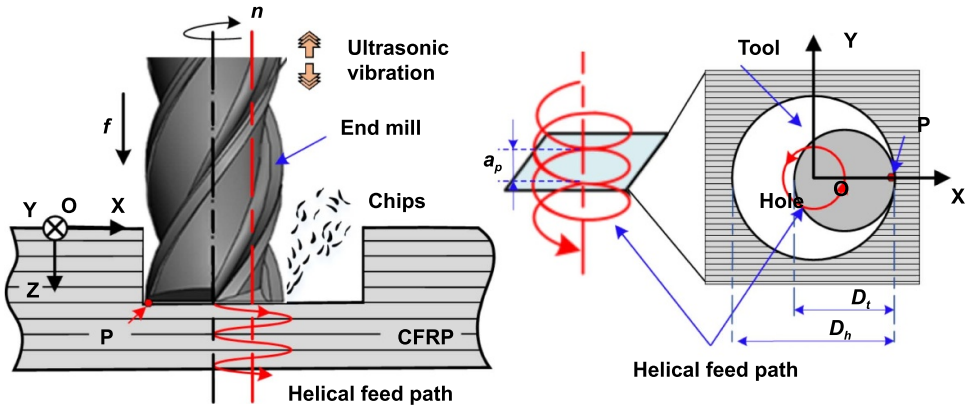

Figure 2. Schematic illustration of WMM.

2. Methods and experimental procedures

2.1. The principle of WMM

As a novel process, WWM applies an axial ultrasonic vibration on the cutting edges while the end mill rotates along its own axis and helical feeds into the workpiece, as shown in figure 2. The O-*XYZ* was established as a workpiece coordinate system. The relation between the instantaneous position of a random point 'P' on the cutting edge and cutting time t can be expressed as follows:

$$\begin{cases} x = \frac{D_h - D_t}{2}\cos\left(\frac{2\pi n_t t}{60}\right) + R\cos\left(\frac{2\pi n_s t}{60}\right) \\ y = \frac{D_h - D_t}{2}\sin\left(\frac{2\pi n_t t}{60}\right) + R\sin\left(\frac{2\pi n_s t}{60}\right) \\ z = -a_p n_t t + A\sin(2\pi f t) \end{cases} \quad (1)$$

where D_h is the hole diameter, D_t is the tool diameter, n_t is the tool helical revolution speed, R is the radius of point P, n_s is the spindle speed, a_p is the axial feed per helical revolution, A and f are the amplitude and frequency of ultrasonic vibration, respectively.

Figures 3(a) and (b) show the motion trajectories of point P in WMM and CHM obtained with MATLAB software. No obvious differences were found between the macro-scale trajectories (figure 3(a)) for WMM and CHM. However, the magnified view (figure 3(b)) shows that the motion trajectory of cutting edge in WMM changes periodically in wave-like curve as opposed to the standard arc seen in CHM. The interaction between the motion trajectories of the cutting edges leads to the periodic contact and separation between the tool and workpiece in WMM (i.e. wave-motion cutting mode). According to Sui *et al* [16], the wave-motion cutting mode can be achieved in WMM when the cutting parameter reaches $f_z \leqslant 2A\left|\sin\left((W_\mathrm{f}/2)\pi\right)\right|$, where f_z indicates feed per tooth and W_f refers to the vibration frequency and rotation speed of the tool. In terms of material removal, the front cutting edges in WMM involve cutting duration and separating duration, as shown in figure 3(c), which reduces the thrust force and cutting temperature. The wave-motion cutting mode obtained in WMM also occurs in high-speed ultrasonic vibration cutting [16, 18, 19].

2.2. Materials, experimental setup and conditions

In this study, a 10 mm thick CFRP plates provided by Chengdu Aircraft Industrial (Group) Co., Ltd was used. All CFRP plates were made from an epoxy-based matrix and carbon fabric pre-pregs with 54 unidirectional plies laid up according to an orientation of [0°/−45°/45°/90°]s, as shown in figure 4. The high tensile

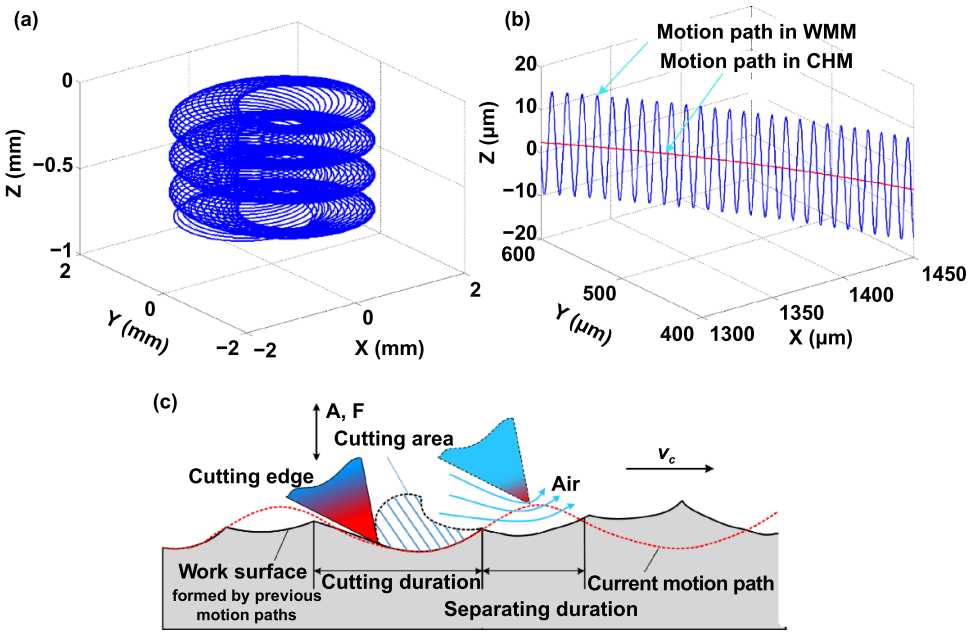

Figure 3. (a) Macro-scale trajectories of point P and (b) partial magnified view in both WMM and CHM, and (c) wave-motion cutting mode in WMM.

Figure 4. The CFRP specimens.

strength pre-pregs were 0.18 mm in thickness. Uncoated carbide end mills with a threaded shank, four teeth, and a diameter of 6 mm were used to process 9 mm holes.

The experimental setup is showed in figure 5. The BV100 vertical machining center, supplied by Beijing electromechanical Machine Tool Co., Ltd, with a self-designed WMM unit was used in the experiments. The WMM unit consisted of an ultrasonic shank, piezoelectric transducer, and carbide end mill with a threaded shank. In the experiment, the piezoelectric transducer was driven and controlled by an ultrasonic power supply. Under no-load conditions, the amplitude at the cutting edges measured by a laser micrometer system (LK-H020, KEYENCE) varied from 6 to 14 μm, according to the input ultrasonic power. The amplitude was set at 10 μm. A piezoelectric dynamometer (Kistler 9272A) was used to measure the cutting force during CFRP hole-manufacturing. The sampling rate was set at 1000 Hz.

In the present work, the surface roughness of the machined CFRP holes was measured by the Talysurf 50 surface tester with an evaluation length of 8 mm and cut-off length of 0.8 mm. In order to alleviate the adverse effects of fiber direction on surface roughness, eight measurements were executed, and the results were averaged, as shown in figure 6.

In this study, both axial feed per tooth (f_{za}) and tangential feed per tooth (f_{zt}) were considered in both WMM and CHM. According to the kinematics within the process, the axial feed per tooth (f_{za}) and tangential feed per tooth (f_{zt}) can be expressed as:

$$f_{za} = \frac{a_{\mathrm{p}} n_{\mathrm{t}}}{m n_{\mathrm{s}}} \tag{2}$$

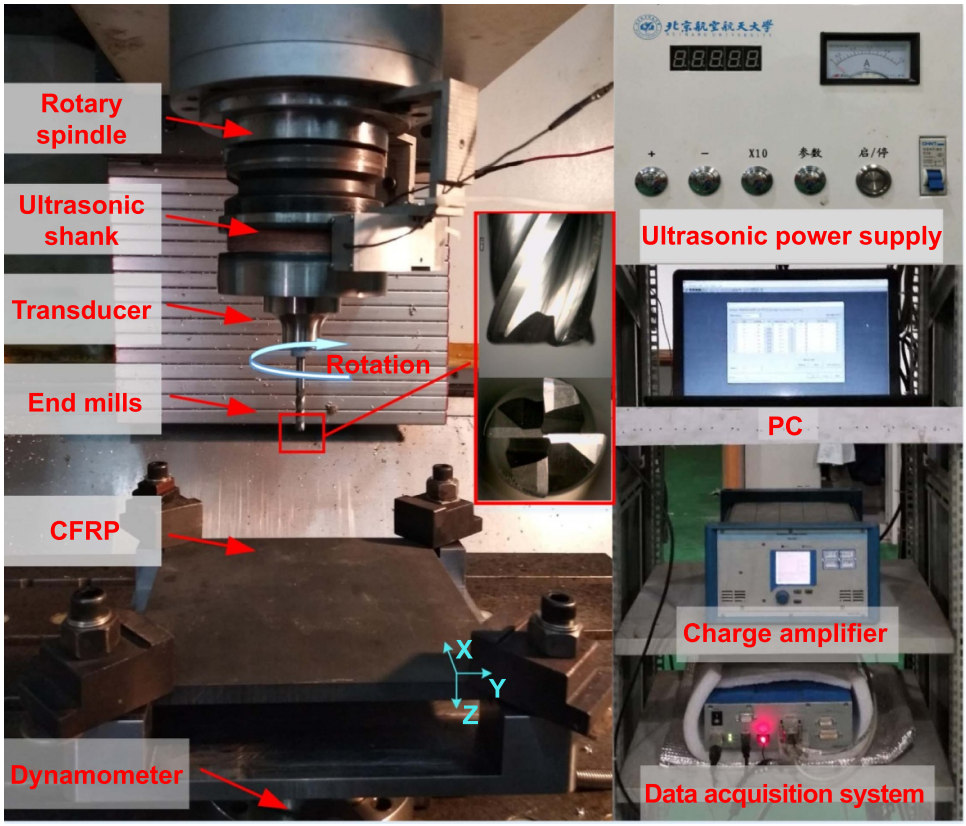

Figure 5. Experimental setup.

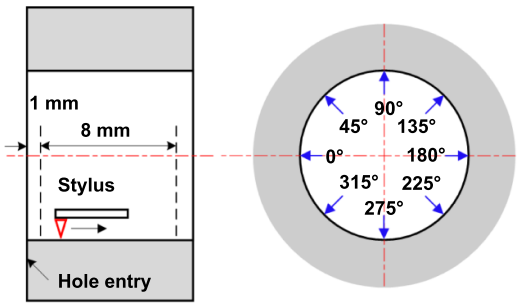

Figure 6. The schematic illustration of surface roughness measurement.

$$f_{zt} = \frac{\pi n_{\mathrm{t}} \left(D_{\mathrm{h}} - D_{\mathrm{t}}\right)}{m n_{\mathrm{s}}}. \tag{3}$$

The revolution speed (f_t) can be expressed as:

$$f_t = \pi n_{\mathrm{t}} \left(D_{\mathrm{h}} - D_{\mathrm{t}}\right). \tag{4}$$

Therefore, the axial feed per tooth (f_{za}) and tangential feed per tooth (f_{zt}) can be changed by the axial feed per helical revolution (a_{p}) and the revolution speed (f_t).

In order to evaluate the feasibility of WMM of CFRP hole, three groups of experiments were conducted, including surface integrity, hole exit damage, and tool wear experiments. All experimental parameters are listed in tables 1–3, respectively. Each experiment was conducted three times.

Table 1. Cutting conditions.

No.	n_s (r min^{-1})	f_t (mm min^{-1})	a_p (mm r^{-1})	f_{zt} (mm r^{-1})	f_{za} (μm r^{-1})	A (μm)	F (kHz)
1	3000	240	0.19	0.02	0.4	6	28.5
2	3000	240	0.28	0.02	0.6	6	28.5
3	3000	240	0.38	0.02	0.8	6	28.5
4	3000	300	0.15	0.025	0.4	6	28.5
5	3000	360	0.13	0.03	0.4	6	28.5
6	3000	240	0.19	0.02	0.4	0	0
7	3000	240	0.28	0.02	0.6	0	0
8	3000	240	0.38	0.02	0.8	0	0
9	3000	300	0.15	0.025	0.4	0	0
10	3000	360	0.13	0.03	0.4	0	0

Table 2. Cutting conditions.

No.	n_s (r min^{-1})	f_t (mm min^{-1})	a_p (mm r^{-1})	f_{zt} (mm r^{-1})	f_{za} (μm r^{-1})	A (μm)	F (kHz)
1	3000	360	0.4	0.03	1.28	6	28.5
2	3000	360	0.6	0.03	1.92	6	28.5
3	3000	360	0.8	0.03	2.56	6	28.5
4	3000	360	0.4	0.03	1.28	0	0
5	3000	360	0.6	0.03	1.92	0	0
6	3000	360	0.8	0.03	2.56	0	0
7	3000	120	0.94	0.01	1	6	28.5
8	3000	240	0.47	0.02	1	6	28.5
9	3000	360	0.31	0.03	1	6	28.5
10	3000	120	0.94	0.01	1	0	0

Table 3. Cutting conditions.

No.	n_s (r min^{-1})	f_t (mm min^{-1})	a_p (mm r^{-1})	A (μm)	F (kHz)
1	3000	360	0.2	6	28.5
2	3000	360	0.2	0	0

3. Results and discussions

3.1. Hole surface quality

Figure 7 shows the representative SEM pictures of the inner surfaces of the holes in both WMM and CHM at the same cutting parameters ($n = 3000$ r min^{-1}, $f_t = 360$ mm min^{-1}, $a_p = 0.3$ mm r^{-1}). According to the previous study on drilling of unidirectional CFRP, fiber orientation angle (i.e. the angle between fiber direction and cutting speed direction) has a significant influence on fiber fractures, which influence the surface quality of machined holes. In figure 6, the hole surface texture with a fiber orientation angle at 0°–180°, 45°, and 90° were observed and compared, respectively. It could be seen that compared with CHM, for a relatively flat fiber fracture with a full, uniform matrix, no obvious fiber breakage phenomenon occurred in WMM. This indicates that the WMM process can achieve superior hole inner surface quality. This result may be due to the ultrasonic oscillatory movement of periphery cutting edges in WMM. Vibratory rubbing and repetitive cutting on the machined surface can smooth the morphology heights of the machined surface. The ultrasonic action of of the front cutting edges of the end mill with high frequency and low amplitude could enhance the cutting ability of the front cutting edges and prompt local fractures of carbon fibers in CFRP [5, 20, 21].

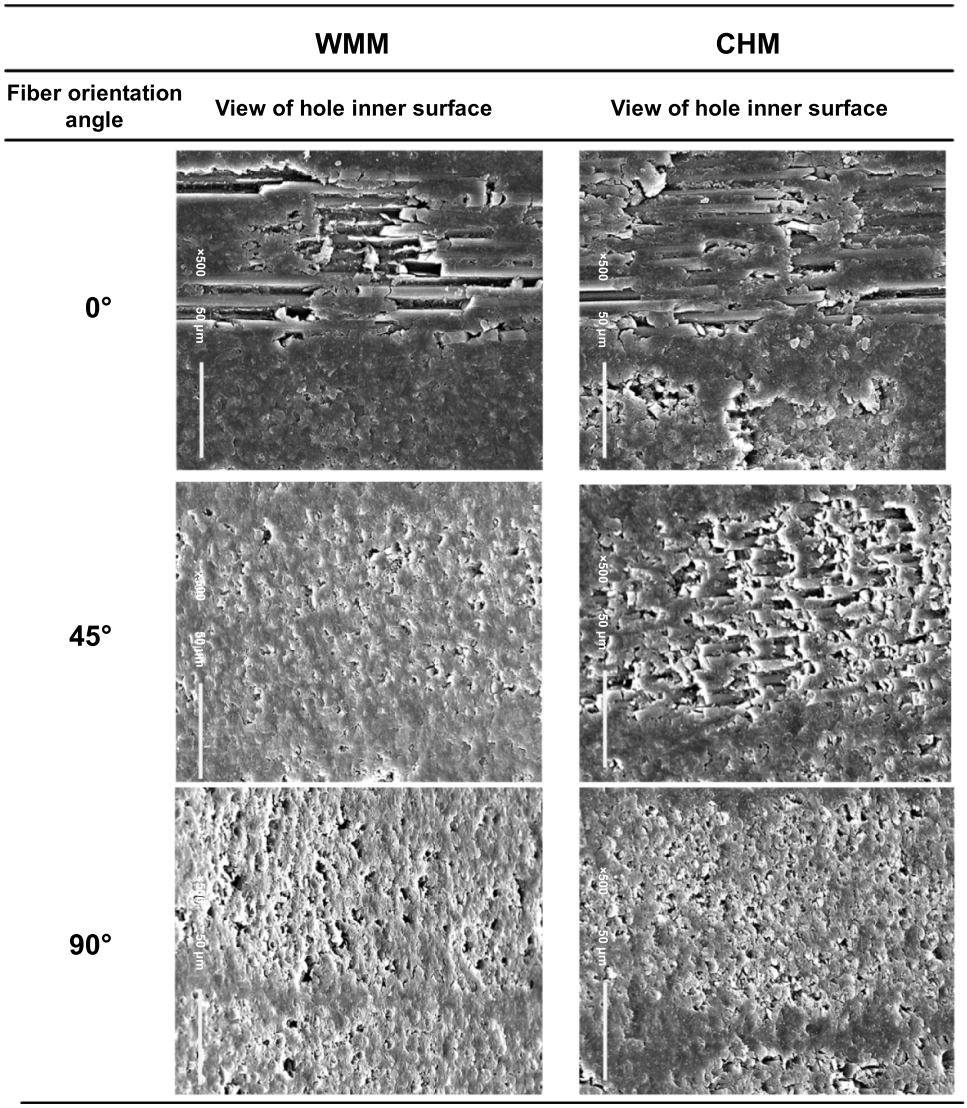

Figure 7. Representative SEM pictures of hole inner surface in both RWMM and CHM at $n_s = 3000$ r min^{-1}, $f_t = 360$ mm min^{-1}, $a_p = 0.3$ mm r^{-1}.

Figure 8 shows the hole inner surface roughness (Ra value) with respect to axial feed per tooth (f_{za}) and tangential feed per tooth (f_{zt}) at a fixed tool rotation speed ($n_s = 3000$ r min^{-1}) in both WMM and CHM. It is clear that the Ra values of machined hole surface in both WMM and CHM increase with increasing axial and tangential feed per tooth. The Ra values of machined hole surface in WMM are smaller than those in CHM with a decrease of 18.1%–36% at all experimental parameters. This indicates that WMM can properly increase each tooth feed to improve machining efficiency while meeting the quality requirements of the hole wall.

3.2. *Analysis of hole exit damage*

In CFRP, hole-manufacturing, delamination and tearing at hole exit are among the most challenging and undesirable failure modes, especially without backup support behind the workpiece. Applying backup support behind the workpiece creates an opposite force, which effectively enhances the critical thrust force of delamination formation [22]. There are few in-depth reports on delamination and tearing at hole exit in the previous studies. However, the support plate is not suitable for workpieces with complex geometries or low accessibility. Therefore,

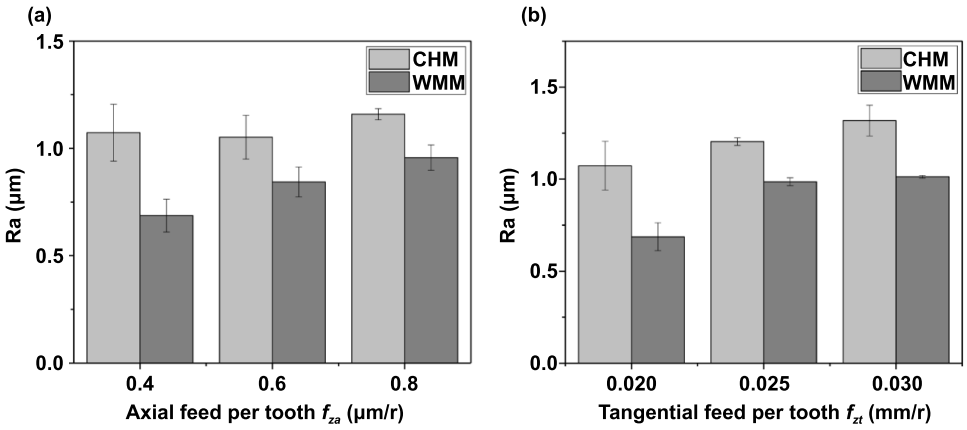

Figure 8. (a) The Ra value with respect to (a) axial feed per tooth (f_{za}) and (b) tangential feed per tooth (f_{zt}) in both WMM and CHM.

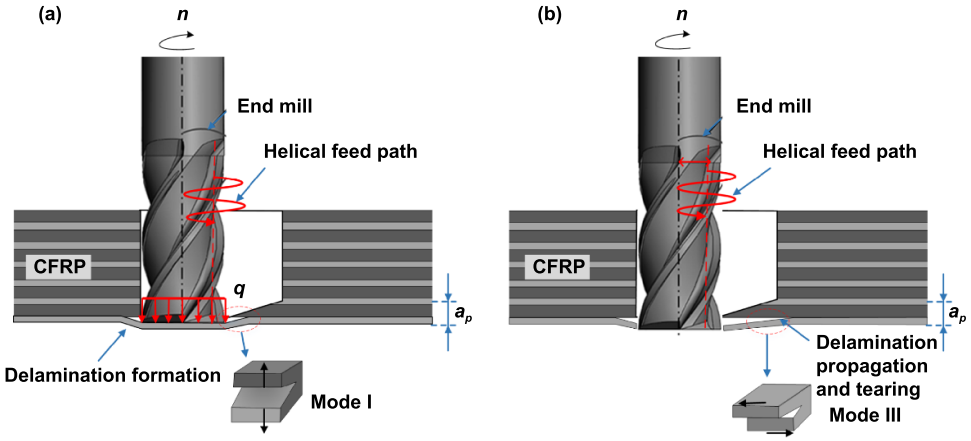

Figure 9. Delamination and tearing formation mechanism.

the delamination and tearing formation mechanism in both WMM and CHM without back support should be further analyzed in detail. Moreover, in this section, the thrust force, delamination, and tearing damage at the hole exit with cutting parameters in both WMM and CHM were measured and discussed.

3.2.1. Mechanism of delamination and tearing formation. As shown in figure 9, during the CHM of CFRP, an eccentric distributed load q from the front surface of the end mill acts on the uncut plies beneath the front of the tool surface. Deformation occurs much easier when using thinner uncut plies. When the vertical stress exceeds the interlayer bonding strength of CFRP laminates, the push-out delamination resulted from Mode I opening cracks appears. Delamination at the hole exit propagates when the tool penetrates the CFRP laminates. As the tool penetrates the workpiece, the side edges of the tool remove the furthest uncut fibers with a maximum height of axial feed per helical revolution (a_p). Therefore, the delamination propagates further, resulting in Mode III tearing cracks. The formation mechanism of delamination and tearing in the tool penetrates the workpiece is similar to that at the workpiece top surface in conventional side milling [23].

3.2.2. Thrust force. Figure 10 shows the thrust forces with respect to axial feed per tooth (f_{za}) and tangential feed per tooth (f_{zt}) in both WMM and CHM. In figure 10(a), it can be seen that in CHM, the thrust force increases as axial feed per tooth increases. Conversely, no obvious variation trend can be found in

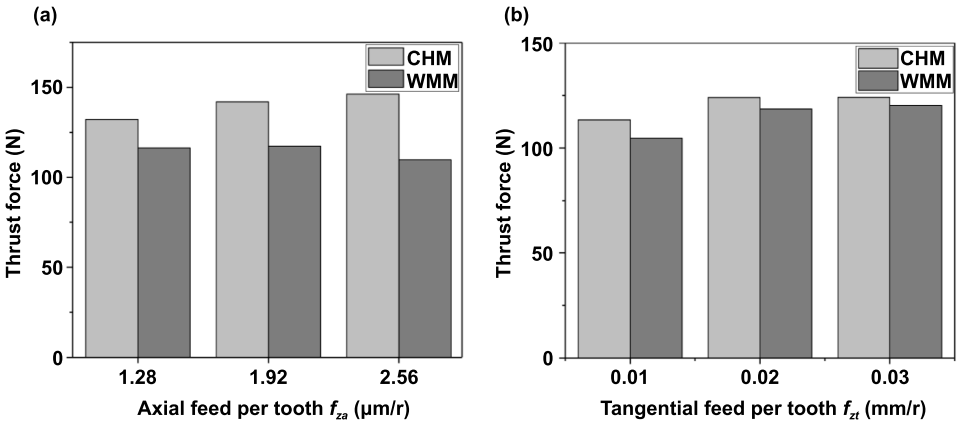

Figure 10. Thrust forces with respect to (a) axial feed per tooth (f_{za}) and (b) tangential feed per tooth (f_{zt}) in both WMM and CHM.

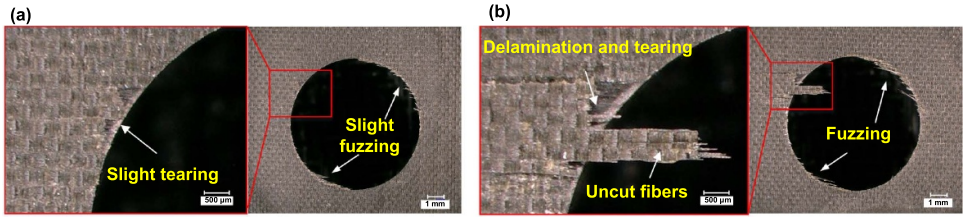

Figure 11. Hole exit morphologies achieved by (a) WMM and (b) CHM with $n_s = 3000$ r min^{-1}, $f_t = 360$ mm min^{-1}, $a_p = 0.8$ mm r^{-1}.

WMM. Moreover, thrust force in WMM was much smaller with a reduction of 12.0%–24.9% at different axial feed per tooth compared to that in CHM. The results of thrust force reduction were also reported by Li *et al* [24] in ultrasonic assisted drilling of titanium alloy and by Geng *et al* [25] in ultrasonic assisted grinding of CFRP. The remarkable decrease in thrust force can be attributed to the wave-motion cutting mode for front cutting edge. In figure 10(b), at the constant axial feed per tooth, the thrust force variation with increasing tangential feed per tooth is not that obvious. Moreover, the thrust force in WMM decreases by only 3%–7.7% at different tangential feed per tooth compared to CG, indicating that the axial feed per tooth is the key parameter affecting thrust force. This is because the front edges of the end mill remove more material than the side edges. The axial force primarily comes from the front cutting edge, according to Brinksmeier *et al* [26].

3.2.3. Hole exit damage. The representative hole exit morphologies achieved in both WMM and CHM without the backup support are shown in figure 11. It can be seen that the hole exit damages in the form of uncut fibers, delamination, and tearing and fuzzing were observed in CHM, but only slight tearing and fuzzing were observed in WMM. These findings indicate that WMM can effectively alleviate hole exit damage.

Figure 12 shows the average tear length at hole exit related to processing parameters in WMM and CHM. The average tear lengths obtained in CHM exceed 1.5, indicating that significant delamination and tearing damage can be induced in CHM without backup support. Moreover, figure 12 shows that the average tear length in both WMM and CHM decreased with increasing axial feed per tooth and increased when tangential feed per tooth increased. Faraz *et al* [27] reported that the delamination and tear size increased with increasing thrust force during twist drilling of CFRP. However, figures 10 and 12 in the present work show that changes in the average tear length did not coincide with the changes in

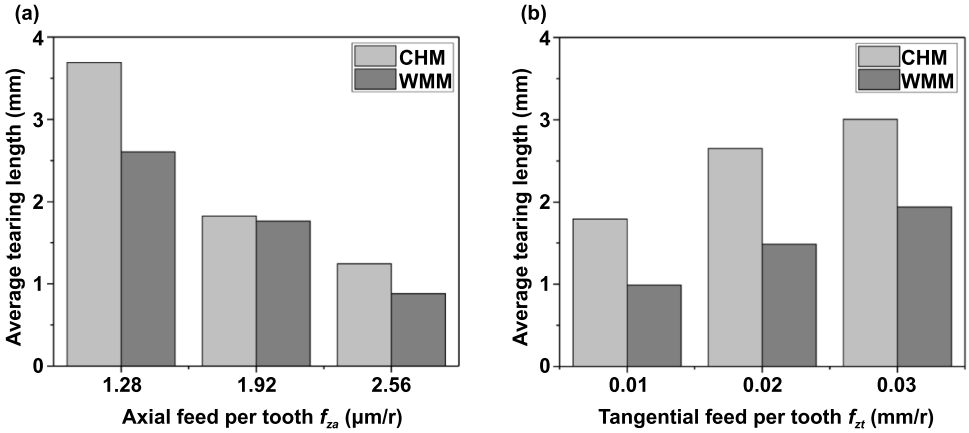

Figure 12. Average tearing length with respect to (a) axial feed per tooth (f_{za}) and (b) tangential feed per tooth (f_{zt}) in both WMM and CHM.

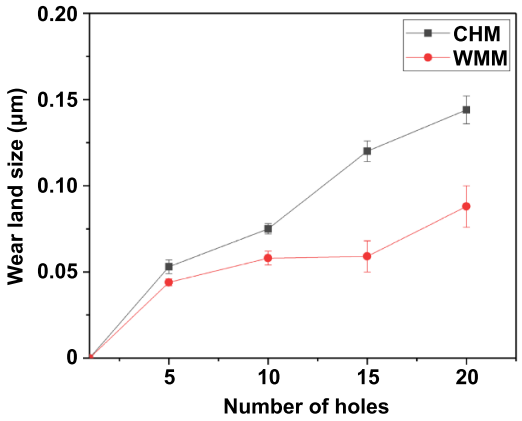

Figure 13. Wear land size of front cutting edges of end mill for various holes in both WMM and CHM.

thrust force with axial feed per tooth and tangential feed per tooth. This indicates that the thrust force in CHM of CFRP was not the main factor inducing hole exit delamination and tearing. Using formulas (2) and (3), it can be found that axial feed per helical revolution (a_p) is directly proportional to the axial feed per tooth and inversely proportional to the tangential feed per tooth, indicating that the average tear length in either WMM or CHM decreases with increasing helical revolutions. Therefore, the formation and propagation of delamination and tearing in WMM of CFRP is more complicated than in conventional twist drilling, induced by the thrust force and axial feed per helical revolution (a_p). To better understand the basic principles of delamination and tearing, further research should be carried out in the future.

It can be also seen from figure 12 that, compared to those in CHM, the average tear lengths in WMM are 3.5%–29.5% smaller at different axial feed per tooth and 35.5%–44.7% smaller at tangential feed per tooth. Based on a previous analysis, the significant reduction of thrust force in WMM suppresses hole exit delamination and tearing.

3.3. Tool wear observation

Figure 13 shows the wear situations on the front edges of the end mill for various holes in both WMM and CHM at the same cutting parameters ($n = 3000$ r min^{-1}, $f_t = 360$ mm min^{-1}, $a_p = 0.2$ mm r^{-1}). It can be seen that with the same number of holes, the tool wear situations in WMM are superior to those in CHM. After machining five holes, the wear land size of the flank face of the WMM front edge

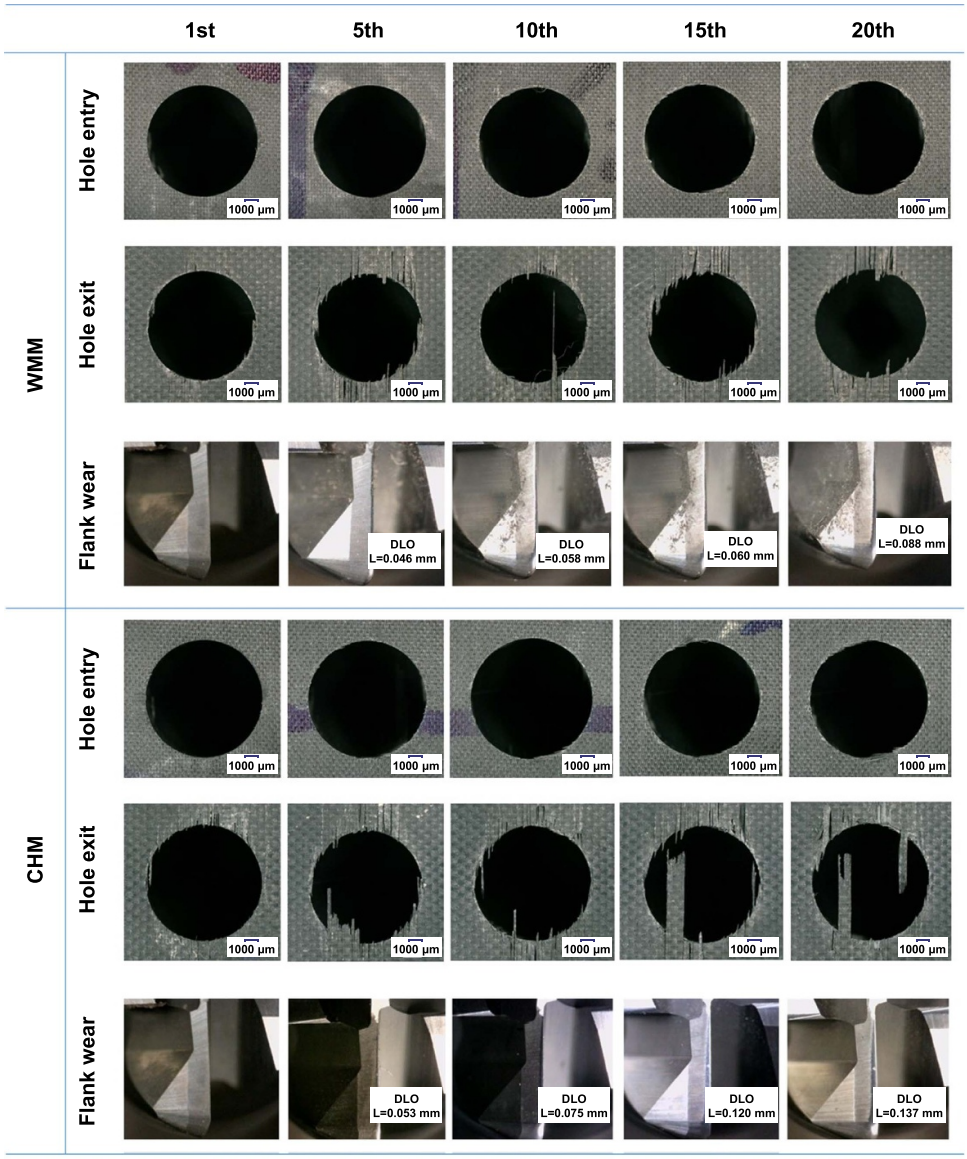

Figure 14. Morphologies of hole entry and exit corresponding to the different tool wear conditions at $n_s = 3000$ r min^{-1}, $f_t = 360$ mm min^{-1}, $a_p = 0.2$ mm r^{-1}.

was 0.046 mm, similar to the 0.053 mm wear land size in CHM. Machining more holes reveals more noticable differences in tool wear situations between WMM and CHM. After machining 10 holes, the wear land size in CHM had reached 0.075 mm, with only 0.058 mm in WMM. After machining 15 holes, the wear area in CHM was twice that in WMM (0.12 mm vs. 0.06 mm). The sharp increase of wear from 0.075 mm to 0.12 mm in CHM indicated that the tool had been severely worn from machining the 10th hole to the 15th hole. While in WMM, the wear size of 0.06 mm remained stable between machining 10 holes to 15 holes, indicating that the tool was in a stable wear stage. After machining 20 holes, the wear size in WMM was 0.088 mm, a significant increase compared with that in 15 holes, indicating that the tool started to wear. The wear size for CHM after machining 20 holes reached 0.146 mm, significantly higher than that in WMM. This indicates that WMM can significantly prolong the tool life, compared to CHM. By alleviating tool wear, WMM could, to a certain extent, increase cutting speed as well as hole manufacturing efficiency.

Figure 14 shows that the morphologies of hole entry and exit corresponding to the different tool wear conditions at ($n_s = 3000$ r min^{-1}, $f_t = 360$ mm min^{-1},

$a_p = 0.2$ mm r^{-1}). It is clear that compared with hole exit morphologies, the quality of the hole entry was significantly improved. For the hole entry, the first hole in either WMM or CHM was basically free of burrs. However, the continuous tool wear led to more obvious the burrs appeared. For the hole exit, obvious delamination and tearing defects were observed in both WMM and CHM. Moreover, the defects became more server with continuous tool wear.

4. Conclusion

This paper presents evaluated the feasibility of WMM of CFRP hole under dry conditions. The hole quality and tool wear in both WMM and CHM were compared and analyzed. The experimental results suggest that WMM is a proper and promising strategy for CFRP hole-manufacturing. The main conclusions can be drawn as follows:

(a) The motion trajectory of the WMM cutting edge was modelled and analyzed. Compared to the standard curve in CHM, the motion trajectory curve in WMM periodically changed, indicating that the wave-motion cutting mode can be achieved by front cutting edges in WMM rather than continuous cutting in CHM.

(b) Compared to CHM, superior hole surface integrity was achieved in WMM. The relatively flat fiber fracture in full and uniform matrix with no obvious fiber breakage being observed in WMM. WMM achieved much smoother hole surfaces, which resulted in a 18.1%–36% decrease in the Ra value under same conditions. This can be attributed to the axial high-frequency oscillatory movement of the peripheral cutting edges and the ultrasonic impact action of the front cutting edges.

(c) Thrust force in WMM was much lower than that in CHM with a reduction of 12.0%–24.9% for different axial feed per tooth and 3%–7.7% for different tangential feed per tooth. This indicates that the intermittent cutting mode of the front cutting edges is the main reason for the reduction of thrust force.

(d) The delamination, tearing, and uncut fiber bundles at the hole exit were obviously alleviated in WMM, compared to CHM. Hole exit damages in the form of uncut fibers, delamination and tearing, edge chipping and fuzzing were found in CG, while only slight edge chipping, fuzzing, and tearing were found in WMM. The average tear lengths in WMM were shorter than those in CHM with a decrease of 3.5%–29.5% at different axial feed per tooth and with a decrease of 35.5%–44.7% at tangential feed per tooth.

(e) The tool wear in WMM is obviously superior to that in CHM. After machining 20 holes, the wear land size in WMM was 0.088 mm and 0.146 mm in CHM.

Acknowledgments

This work was supported by National Natural Science Foundation of China (Grant Nos. 51905024, 51905138, 51975035 and 91960203).

ORCID iD

Daxi Geng https://orcid.org/0000-0003-3591-4630

References

[1] Yashiro T, Ogawa T and Sasahara H 2013 Temperature measurement of cutting tool and machined surface layer in milling of CFRP *Int. J. Mach. Tools Manuf.* **70** 63–9

[2] Díaz-Álvarez J, Olmedo A, Santiuste C and Miguelez M H 2014 Theoretical estimation of thermal effects in drilling of woven carbon fiber composite *Materials* **7** 4442–54

[3] Geng D X, Lu Z H, Yao G, Liu J J, Li Z and Zhang D Y 2017 Cutting temperature and resulting influence on machining performance in rotary ultrasonic elliptical machining of thick CFRP *Int. J. Mach. Tools Manuf.* **123** 160–70

[4] Wang J J, Feng P F, Zhang J F and Shen H 2017 Experimental investigation on the effects of thermomechanical loading on the vibrational stability during rotary ultrasonic machining *Mach. Sci. Technol.* **21** 239–56

[5] Cong W L, Pei Z J, Deines T W, Liu D F and Treadwell C 2013 Rotary ultrasonic machining of CFRP/Ti stacks using variable feedrate *Composites* B **52** 303–10

[6] Singh A P, Sharma M and Singh I 2013 A review of modeling and control during drilling of fiber reinforced plastic composites *Composites* B **47** 118–25

[7] Xu J Y and Mansori M E 2016 Experimental study on drilling mechanisms and strategies of hybrid CFRP/Ti stacks *Compos. Struct.* **157** 461–82

[8] Xia T, Kaynak Y, Arvin C and Jawahir I S 2016 Cryogenic cooling-induced process performance and surface integrity in drilling CFRP composite material *Int. J. Adv. Manuf. Technol.* **82** 605–16

[9] Tsao C C and Chiu Y C 2011 Evaluation of drilling parameters on thrust force in drilling carbon fiber reinforced plastic (CFRP) composite laminates using compound core-special drills *Int. J. Mach. Tools Manuf.* **51** 740–4

[10] Chen W C 1997 Some experimental investigations in the drilling of carbon fiber-reinforced plastic (CFRP) composite laminates *Int. J. Mach. Tools Manuf.* **37** 1097–108

[11] Wang H, Pei Z J and Cong W L 2020 A feeding-directional cutting force model for end surface grinding of CFRP composites using rotary ultrasonic machining with elliptical ultrasonic vibration *Int. J. Mach. Tools Manuf.* **152** 103540

[12] Wang H, Pei Z J and Cong W L 2020 A mechanistic cutting force model based on ductile and brittle fracture material removal modes for edge surface grinding of CFRP composites using rotary ultrasonic machining *Int. J. Mech. Sci.* **176** 105551

[13] Ning F D, Cong W L, Pei Z J and Treadwell C 2016 Rotary ultrasonic machining of CFRP: a comparison with grinding *Ultrasonics* **66** 125–32

[14] Cong W L, Feng Q, Pei Z J, Deines T W and Treadwell C 2012 Rotary ultrasonic machining of carbon fiber-reinforced plastic composites: using cutting fluid vs. cold air as coolant *J. Compos. Mater.* **46** 1745–53

[15] Feng Q, Cong W L, Pei Z J and Ren C Z 2012 Rotary ultrasonic machining of carbon fiber-reinforced polymer: feasibility study *Mach. Sci. Technol.* **16** 380–98

[16] Sui H, Zhang X Y, Zhang D Y, Jiang X G and Wu R B 2017 Feasibility study of high-speed ultrasonic vibration cutting titanium alloy *J. Mater. Process. Technol.* **247** 111–20

[17] Geng D X, Liu Y H, Shao Z Y, Zhang M L, Jiang X G and Zhang D Y 2020 Delamination formation and suppression during rotary ultrasonic elliptical machining of CFRP *Composites* B **183** 107698

[18] Liu J J, Jiang X G, Han X and Zhang D Y 2018 Influence of parameter matching on performance of high-speed rotary ultrasonic elliptical vibration-assisted machining for side milling of titanium alloys *Int. J. Adv. Manuf. Technol.* **101** 1333–48

[19] Zhang X Y, Sui H, Zhang D Y and Jiang X G 2018 Study on the separation effect of high-speed ultrasonic vibration cutting *Ultrasonics* **87** 166–81

[20] Shao Z Y, Jiang X G, Zhang D Y, Geng D X, Li S M and Liu D P 2019 Defect suppression mechanism and experimental study on rotary ultrasonic-assisted drilling of CFRP *J. Beijing Univ. Aeronaut. Astronaut.* **45** 1613–21

[21] Geng D X, Liu Y H, Shao Z Y, Lu Z H, Cai J, Li X, Jiang X G and Zhang D Y 2019 Delamination formation, evaluation and suppression during drilling of composite laminates: a review *Compos. Struct.* **216** 168–86

[22] Tsao C C and Hocheng H 2007 Parametric study on thrust force of core drill *J. Mater. Process. Technol.* **192–193** 37–40

[23] Hintze W, Hartmann D and Schütte C 2011 Occurrence and propagation of delamination during the machining of carbon fibre reinforced plastics (CFRPs)—an experimental study *Compos. Sci. Technol.* **71** 1719–26

[24] Li Z, Zhang D Y, Jiang X G, Qin W and Geng D X 2017 Study on rotary ultrasonic-assisted drilling of titanium alloys (Ti6Al4V) using 8-facet drill under no cooling condition *Int. J. Adv. Manuf. Technol.* **90** 3249–64

[25] Geng D X, Teng Y D, Liu Y H, Shao Z Y, Jiang X G and Zhang D 2019 Experimental study on drilling load and hole quality during rotary ultrasonic helical machining of small-diameter CFRP holes *J. Mater. Process. Technol.* **270** 195–205

[26] Brinksmeier E, Fangmann S and Meyer I 2008 Orbital drilling kinematics *Prod. Eng.* **2** 277–83

[27] Faraz A, Biermann D and Weinert K 2009 Cutting edge rounding: an innovative tool wear criterion in drilling CFRP composite laminates *Int. J. Mach. Tools Manuf.* **49** 1185–96